JOURNAL OF CATALYSIS **172,** 118–126 (1997)
ARTICLE NO. CA971823

Specific Features Concerning the Mechanism of Methane Reforming by Carbon Dioxide over Ni/La_2O_3 Catalyst

A. Slagtern,* Y. Schuurman,† C. Leclercq,† X. Verykios,‡ and C. Mirodatos†,[1]

†*Institut de Recherches sur la Catalyse, CNRS, 2, Avenue Albert Einstein, F-69626, Villeurbanne Cedex, France;* **SINTEF Applied Chemistry, Postboks 124 Blindern, N-0314 Oslo, Norway; and* ‡*Department of Chemical Engineering, University of Patras, Gr-26500 Patras, Greece*

Received March 10, 1997; revised June 27, 1997; accepted June 30, 1997

The reforming of methane by carbon dioxide is studied over a Ni/La_2O_3 catalyst which presents an unusual catalytic stability compared to other nickel-based catalysts. A thorough TEM/EDX study combined with isotopic transient DRIFT and TAP experiments reveals the existence of a tight interface between a lanthanum carbonate phase and the nickel particles. A "bi-functional" mechanism is proposed to account for the observed kinetic behaviour: methane is activated on the Ni particles, carbon dioxide interacts with La_2O_3 to form carbonates which scavenge carbon from nickel at the Ni–La_2O_3 interface, thus restoring the Ni particles to their original state. This specific morphology of the active phase is also assumed to hinder the formation of deactivating coke, which explains the catalytic stability of such a catalyst.

1. INTRODUCTION

It is generally assumed that the active phase for CO_2 reforming of methane over nickel-based catalysts consists of metal particles, as demonstrated for $Ni/La_2O_3/Al_2O_3$ (1), and for Ni/SiO_2 catalysts (2, 3). For the latter case, the active surface was shown to be actually a layer of carbide-like nickel Ni_2C or Ni_3C, partly occupied by O atoms. The carbon and oxygen atoms derived from methane cracking and from the dissociative adsorption of carbon dioxide on the metallic surface, respectively (3). No specific role was attributed to the silica support within the catalytic cycle. However, the metal/support interaction was found to control the nickel dispersion and morphology during the reduction period, which may indirectly affect the side reactions of coke formation (2). In contrast, a major role of the support was postulated by Zhang *et al.* (4–6) for explaining the peculiar catalytic behaviour observed over Ni/La_2O_3 catalysts. As a matter of fact, this type of catalyst was found to present unique stability with time on stream, preceded by an activation period of about 4 h, while other formulas, such as Ni/Al_2O_3, Ni/CaO, $Ni/CaO/Al_2O_3$ presenting the same nickel loading (17 wt%) continuously deactivated along the catalytic run (operating conditions: $CH_4/CO_2/He = 20/20/20$ vol%, $T = 750°C$, as reported in Fig. 1 in (5)). Further experiments revealed that the Ni/La_2O_3 catalyst was also found to be stable under reforming conditions when pure components ($CH_4/CO_2 = 1/1$) were used for at least 150 h at 800°C. A slight deactivation has been observed at elevated pressure (10 bar) which can be eliminated by the addition of oxygen or steam in the feed mixture. From FTIR, XPS, and SIMS data, it has been suggested that for this case of Ni/La_2O_3 a lanthanum carbonate phase could prevent the nickel phase to be shielded by carbon deposition (4, 5). This carbonate phase would also participate in the catalytic cycle by providing active species reacting with the carbon species issued from the methane activation on the nickel particles to form CO according to

$$C{-}Ni_n + La_2O_2CO_3 \rightarrow 2CO + Ni_n + La_2O_3.$$

In order to further elucidate these catalytic and mechanistic features, a thorough study by high resolution transmission electron microscopy (TEM) was carried out on the lanthana-supported nickel catalyst, along with *in situ* diffuse reflectance infrared Fourier transform spectroscopy (DRIFT), steady state isotopic transient kinetic analysis (SSITKA), and temporal analysis of product (TAP) investigations.

2. EXPERIMENTAL

2.1. Catalyst Preparation and Testing

Ni/La_2O_3 catalyst. The 17 wt% Ni/La_2O_3 catalyst was prepared by the wet-impregnation method, using nitrate salt as the metal precursor. The La_2O_3 used was of ultra-high purity (Alpha Products). Its surface area is approximately 2 m^2/g. A weighted amount of nickel nitrate (Alfa Products) and of lanthana was placed in a 100-ml beaker and a small amount of distilled water was added under continuous stirring. The slurry was heated to ca 80°C and maintained at that temperature until the water evaporated. The

[1] To whom correspondence should be addressed. E-mail: mirodato @catalyse.univ-lyon1.fr.

0021-9517/97 $25.00

residue was then dried at 110°C for 24 h and was subsequently heated to 500°C under N_2 flow for 2 h for complete decomposition of the nitrate. After this treatment, the catalyst was reduced at 500°C in H_2 flow for 5 h. The resulting catalyst presented a total surface area of 1.2 m^2/g, and the dispersion of Ni was found to be less than 1% from H_2 volumetric data. The size of the catalyst pellets used for reaction was in the range of 0.2–0.3 mm.

The catalyst was activated by exposure to a $CH_4/CO_2/He = 20/20/60$ vol% stream at 750°C for 3 h. After this treatment, the flow rate was adjusted so as to obtain differential (<10%) or integral conversion. The mass of catalyst used in the ageing experiments was typically 30–50 mg, while the feed flow rate was varied between 100 and 500 cm^3/min.

Ni/SiO_2 catalyst. The Ni/SiO_2 catalyst used in this work as a reference catalyst was prepared by wet impregnation of a Degussa Aerosil P200 support with a $Ni(NH_3)_6NO_3$ solution as described in (2). After evaporation, the precursor was dried at 120°C. Calcination of the catalyst was performed *ex situ* under flowing oxygen at 750°C for 8 h. The nickel content was determined to be 4.0 wt%. Reduction was carried out *in situ* at 750°C for 10 h under flowing hydrogen (flowrate 1.2 liter/h, temperature rate 2.5°C/min). The resulting catalyst presented a total surface area of 150 m^2/g, and a dispersion of Ni around 17% from H_2 volumetry, TEM, and magnetic measurements data (2, 3).

2.2 Applied Techniques

Transmission electron microscopy (TEM) investigations were performed on a JEOL JEM 2010 (resolution of 0.19 nm point to point) fitted with an EDX spectrometer (Link-Isis). Chemical analysis by nanoprobes as small as 1 nm can be obtained with this microscope. The samples were ultrasonically dispersed in ethanol and deposited on a holey carbon film supported on a copper grid.

X-ray diffraction (XRD) experiments were performed using a Phillips PW 1050/81 diffractometer with the Cu Kα radiation under standard acquisition conditions. Continuous scans in the range of 2θ from 10 to 80° were used. JCPDS-ICDD standard spectra software was used to determine the phases.

In situ transient infrared spectroscopic experiments were performed using a Nicolet IR 550 instrument, equipped with an *in situ* DRIFT cell from Spectratech connected to a SSITKA setup (7, 8). About 20 mg of catalyst were loaded in the cell and a CO_2/Ar mixture or a reactant mixture $CH_4/CO_2/Ar = 2/2/1$ was passed over the catalyst at different temperatures. Transient experiments were performed in the DRIFT cell by changing abruptly the gas composition containing unlabelled $^{12}CO_2$ to the same gas composition containing labelled $^{13}CO_2$. The gas effluent was analysed on line using a quadrupole mass spectrometer (VG Micromass).

Transient pulse experiments were performed in a TAP-2 reactor system. In a TAP experiment a narrow gas pulse of reactants is introduced in a microreactor which is evacuated continuously. The response of this pulse is detected by a quadrupole mass spectrometer at the reactor exit. The shape of the response reflects diffusion, adsorption, desorption, and reaction, as extensively described by Gleaves *et al.* (9). The main features of the TAP-2 reactor system (Mithra Technologies Inc.) are: (1) four high-speed pulse valves able to deliver 0.25 ms FWHH pulses; (2) a 25.4 mm in length and 4.1 mm in diameter microreactor; (3) a high-throughput liquid nitrogen trapped vacuum system; (4) a slide valve containing a needle valve to switch between high-pressure experiments and vacuum experiments; (5) a quadrupole mass spectrometer located directly underneath the reactor exit; (6) a gas and liquid vapour feed panel to accurately make up blends; (7) a PC-based system for data collection and pulse valve control. Typically, a catalyst charge of 25 mg with a particle size of 0.3–0.4 mm was placed in the centre of the reactor between two layers of 0.3–0.4 mm size quartz particles.

3. RESULTS

3.1. Changes in Catalyst Structure and Morphology upon Reforming and Regeneration

XRD analysis was performed (i) after reduction, (ii) after reforming reaction under integral conditions in the DRIFT cell, and (iii) after regeneration at 700°C under CO_2, then O_2, following exposure to reaction conditions in the DRIFT cell.

The XRD pattern of the reduced Ni/La_2O_3 catalyst shows essentially metallic Ni and $La(OH)_3$ (Fig. 1a). After CO_2 reforming of methane, the catalyst presents the same

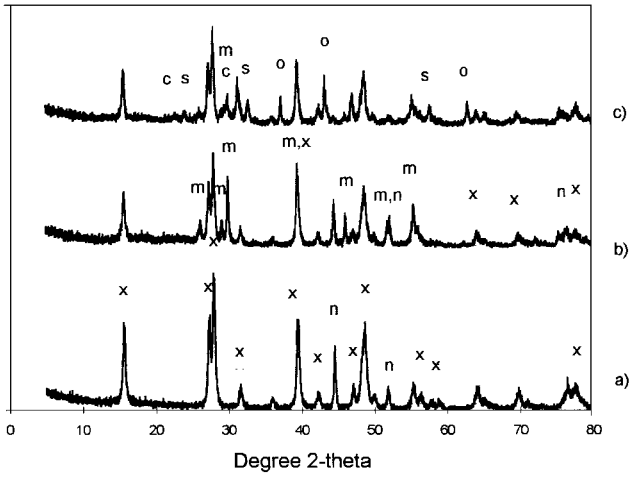

FIG. 1. XRD of Ni/La_2O_3: (a) reduced catalyst stored in air; (b) after burning off coke with CO_2 and O_2; (c) after CO_2 reforming of methane (x = $La(OH)_3$, n = Ni, o = NiO, m = La_2O_3, c = $La_2O_2CO_3$, s = La_2NiO_4).

dark colour as before the test. The XRD pattern shows that along with metallic Ni, $La(OH)_3$ and La_2O_3 phases coexist (Fig. 1b). After a regeneration treatment at 750°C (under CO_2 and O_2, Fig. 1c) the nickel phase is oxidised into NiO. Among the lanthanum based compounds, $La(OH)_3$ and La_2O_3 are still the dominant phases with minor amounts of $La_2O_2CO_3$. In addition, a significant amount of the mixed oxide La_2NiO_4 (and possibly $LaNiO_3$) is unambiguously detected.

TEM investigation was performed (i) after reduction, (ii) after reaction under differential conditions, (iii) after reaction under integral conditions, and (iv) after regeneration by calcination:

(i) On the reduced sample, rather large and faceted Ni particles are observed (50–100 nm), which gives an average Ni dispersion around 1%, in agreement with the volumetric data. Each Ni particle is decorated by a continuous layer of around 2 nm in thickness, as can be seen on Fig. 2A. EDX analyses were carried out on the overlayer (a), on the core of the particle (b), and on the support (c), as reported in Table 1.

TABLE 1

EDX Analysis Carried Out on Various Spots of the Reduced Sample

Area of the EDX analysis	Location in Fig. 2A	La/Ni atomic ratio (%)
Centre of a particle (10 × 10 nm)	b	1/99
Border of a particle (10 × 10 nm)	a	7/93
Border of a particle (5 × 5 nm)	a	12/88
Support area free of particle (10 × 10 nm)	c	100/0

The overlayer which decorates the Ni particles was unambiguously found to contain a significant amount of lanthanum atoms, with the relative amount of La increasing when decreasing the EDX spot size. Indeed, the smallest EDX spot size (5 × 5 nm) being at least 2 times larger than the overlayer (2 nm in thickness), a part of the nickel particle is necessarily included in the analysed area, which explains the large contribution of Ni in the analysis (Table 1).

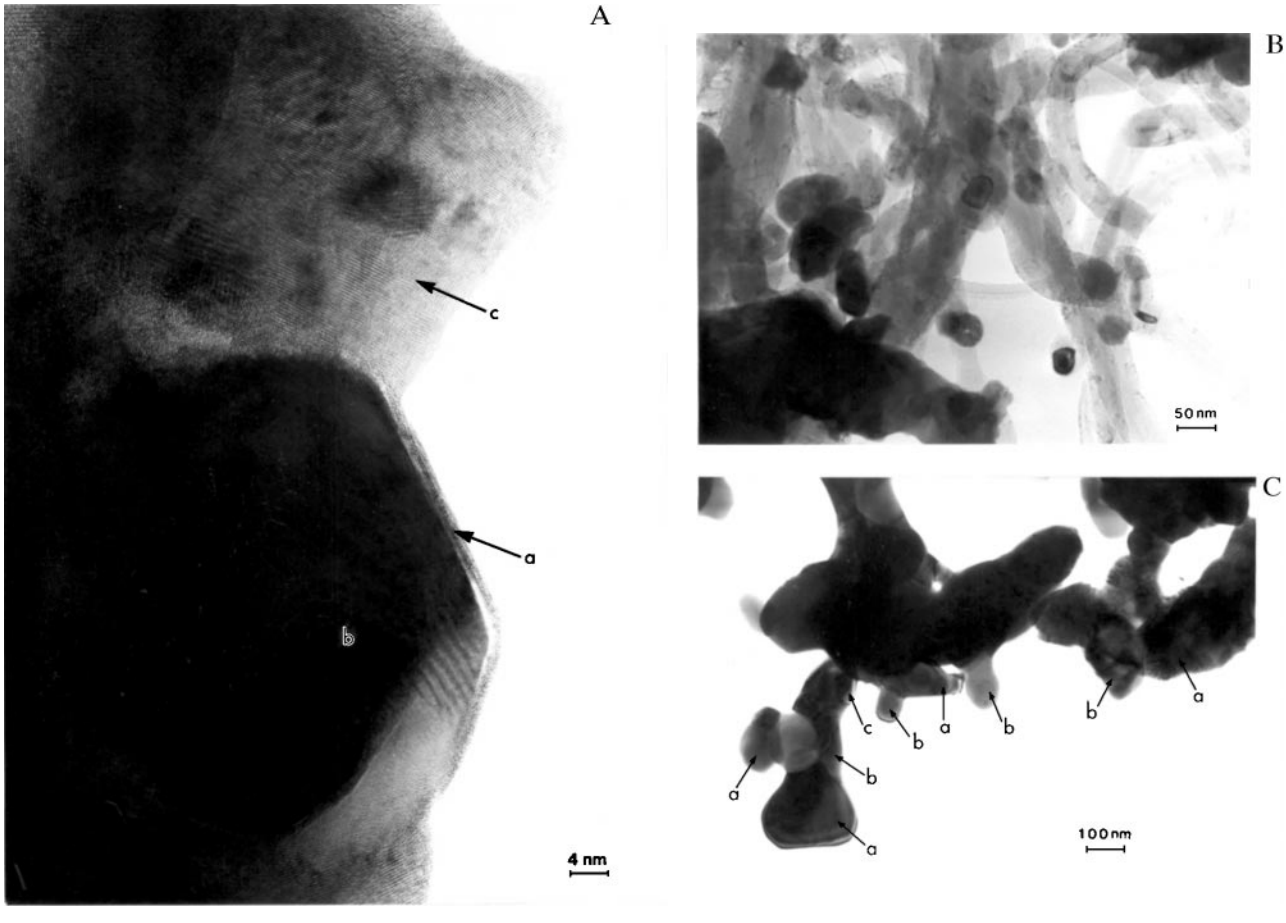

FIG. 2. TEM pictures of Ni/La_2O_3: (A) after initial reduction; (B) after reforming reaction under differential conditions at 750°C; (C) after calcination/regeneration at 750°C.

As seen in Fig. 2A(a), lattice planes of the overlayer are visualised and the crystallographic parameters of this layer, although not easy to measure, are consistent with a lanthanum carbonate structure.

(ii) After 5-min exposure on the reforming stream under differential conditions (conversion about 5%), the decoration of nickel particles is still observed, along with some carbon deposits: veils and hollow filaments, characteristic of the different forms of coke found on nickel catalysts for CO_2 reforming (2).

(iii) After 20-h exposure to the reforming stream, either under differential or integral conditions, most of the Ni particles and lanthana grains appear to be completely surrounded by carbon, which hinders any precise analysis of bulk and surface particle composition. However, the particles present the same average size as the ones of the freshly reduced sample, which discards any significant sintering effect under reaction conditions. It is also observed that some nickel particles have been extracted from the lanthana support by growing filaments, as depicted in Fig. 2B. The lanthanum element is no longer detected by EDX analysis on the border of the extracted particles.

(iv) After regeneration by calcination at 750°C, the catalyst presents a strongly sintered aspect with particles agglomerated together with an average size of around 300–400 nm (Fig. 2C). On this micrograph, EDX analysis reveals zones of pure nickel (a) and zones of mixed lanthanum and nickel composition with two dominant La/Ni atomic ratios around 2 (b) and 1 (c). They probably correspond to the local formation of nickel lanthanum oxides $LaNiO_3$ and La_2NiO_4 as identified by XRD (Fig. 1c). Zones of pure lanthana are observed on other area of similar aspect.

3.2. Characterisation of the Active Surface by DRIFT and Transient Kinetics

Figure 3 reports the DRIFT spectra obtained when heating the reduced sample under Ar flow from 25 to 700°C. It is observed that the OH groups from the initial lanthanum hydroxide phase (3610 and 3450 cm^{-1}) are first shifted to 3595 cm^{-1} for the former groups and then disappear at 700°C, in accordance with the XRD phase transformation to La_2O_3 at high temperature. Carbonate bands are always observed in the range 1300–1500 cm^{-1}, as expected from the highly basic lanthana material, with a transformation from hydroxycarbonate and monodentate carbonate at low temperature to bidentate dioxomonocarbonate $La_2O_2CO_3$ at high temperature (10).

In order to identify the type of interaction between gaseous carbon dioxide and the carbonate phase, a $^{12}CO_2$/Ar (1.5/28.5 ml/min) flowing mixture is passed through the catalyst bed in the DRIFT cell at 700 and 800°C; then it is switched to the equivalent $^{13}CO_2$/Ar + He flowing mixture. The spectra recorded under both isotopic mixtures at 800°C are reported in Fig. 4 (similar spectra were obtained

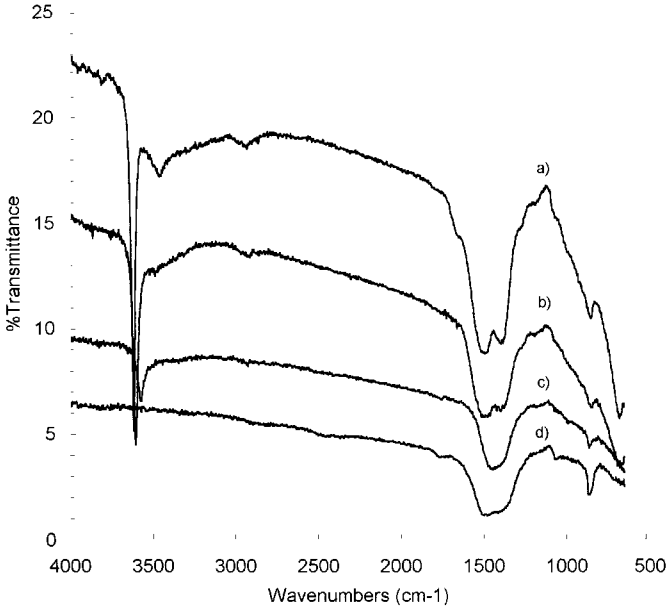

FIG. 3. DRIFT spectra of Ni/La_2O_3 recorded in Ar flow at increasing temperature: (a) 20°C; (b) 300°C; (c) 500°C; (d) 700°C.

at 700°C). In response to the isotopic shift of the gaseous CO_2 (from 2362 to 2298 cm^{-1}) a shift of the whole carbonate bands is noted (from 1508 to 1464 and from 864 cm^{-1} to 836 cm^{-1}). This indicates that all the carbonate species are at equilibrium with the gaseous carbon dioxide at the reforming temperature.

A series of spectra are recorded during the above $^{12}CO_2$/Ar—$^{13}CO_2$/Ar switch (about one spectrum every 5 s) and the gaseous effluent is continuously monitored by mass spectrometry. The normalised changes in the IR band intensity for gaseous $^{12}CO_2$ (2362 cm^{-1}) and for the carbonate adspecies (1508 cm^{-1}) are reported in Fig. 5 (the symmetrical transients observed for the labelled species are not reported for the sake of clarity). A clear shift is observed between the gaseous and the adsorbed CO_2. On the basis of the above finding that an equilibrium exists between the carbon dioxide gas phase and adsorbed carbonates, the normalised response curves of Fig. 5 were modelled by considering a combination of 2 CSTR pools in parallel or in series, according to the formalism developed by Soong *et al.* (11) or Happel *et al.* (12) (Scheme 1).

A first pool (pool 1) represents the gaseous CO_2 phase in the DRIFT cell and a second one (pool 2) represents the adsorbed carbonate phase on the catalyst. This modelling procedure allows us to calculate meaningful parameters: time constant and content of the different pools (8, 11). The model of two pools in parallel (A in the Scheme 1) is found to describe correctly the carbon dioxide gas phase transient, as attested by the fit between the experimental and calculated data (circle symbols and solid line a in Fig. 5). In this model, the transient inlet isotopic step function,

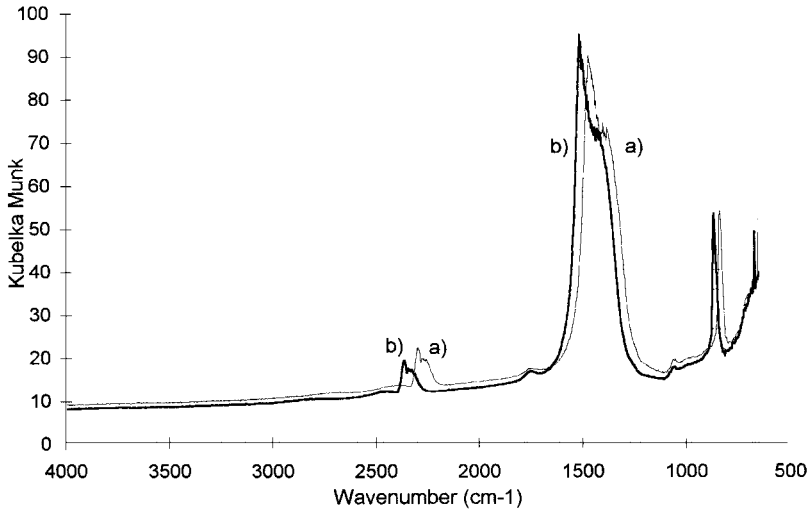

FIG. 4. DRIFT spectra of Ni/La_2O_3 recorded at 800°C: (a) in 5% $^{13}CO_2$/Ar/He flow; (b) in 5% $^{12}CO_2$/Ar/He flow.

represented by the inert gas response, crosses the CO_2 pool with a delay due to the continuous and fast exchange with the carbonate reservoir. A model of two pools in series (model B in Scheme 1) is more adapted to the response of surface CO_3^{2-} groups. This is expected from an isotopic step function first crossing the gaseous pool, then crossing the adsorbed pool to be detected as an outlet function by the infrared analysis of the adsorbed phase (square symbols and solid line b in Fig. 5). From the calculated parameters of the models, pool 2 which is ascribed to the accumulation of exchangeable CO_3^{2-} groups is found to be about 300 μmol/g_{cat}. The total concentration of lanthana in the catalyst is 2546 μmol/g_{cat}, which means that about a tenth of the solid is carbonated under the prevailing conditions. The dispersion of the lanthanum oxide phase can be estimated on the basis of a crystallographic model developed for lanthanum oxide by Lacombe *et al.* (10). Accounting for a measured surface area of 1.2 m^2/g, a dispersion of about 0.5% is determined. On this basis, the concentration of surface lanthana can be evaluated to be 13.5 μmol/g_{cat}. Considering that the carbonates formed are essentially $La_2O_2CO_3$, it can be deduced from the above transient experiments that at 700–800°C and under the partial pressure of CO_2, typical of reforming reaction conditions, approximately 23 monolayers of the

Model A

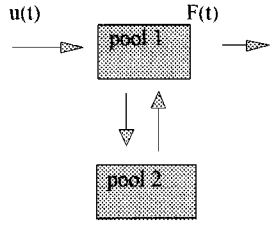

inlet function:

$$u(t) = \exp(-at) / 1 + \exp(-at)$$

outlet function :

$$F(t) = \left[A\exp(-t/\tau_\alpha) + (1-A)\exp(-t/\tau_\beta)\right]u(t)$$

$$A = (1-\tau_1/\tau_\beta)/\tau_1(1/\tau_\alpha - 1/\tau_\beta)$$

Model B

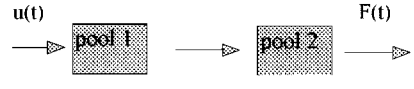

inlet function :

$$u(t) = \exp(-at)/1 + \exp(-at)$$

outlet function :

$$F(t) = [\tau_1/(\tau_1 . \tau_2)\exp(-t/\tau_1) - \tau_2/(\tau_1 - \tau_2)\exp(-t/\tau_2)]\,u(t)$$

SCHEME 1

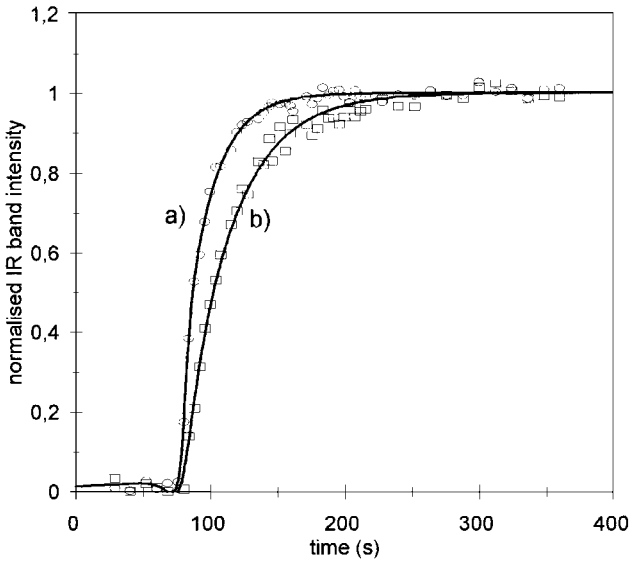

FIG. 5. Normalised changes in the IR band intensity after the $^{13}CO_2$/Ar/He-to-$^{12}CO_2$/Ar switch at 800°C for (a) gaseous $^{12}CO_2$ (2362 cm^{-1}) and (b) carbonate adspecies (1508 cm^{-1}). Modelled curves are the solid lines.

lanthana phase are carbonated and are in equilibrium with the gaseous CO_2. This picture of a rather thick layer of exchangeable carbonates is in good agreement with the complete isotopic shift in IR wavenumbers observed in Fig. 4.

In order to analyse the state of the surface under the reforming reaction conditions, the reacting mixture $^{12}CH_4/^{12}CO_2/Ar$ (1.5/1.8/27 ml/min) is first admitted at 800°C in the catalytic DRIFT cell maintained under He flow. Within one minute, amounts of coke are found to form on top of the catalyst bed, which prevents any precise infrared analysis. This coke formation may be ascribed to severe temperature gradients within the bed induced by the IR window cooling system. However, it is checked by the on-line gas analysis at the reactor outlet that a steady-state activity is maintained, which corresponds to around 20% conversion of both methane and carbon dioxide. The SSITKA experiments corresponding to a switch at 800°C from $^{12}CH_4/^{12}CO_2/Ar$ to $^{12}CH_4/^{13}CO_2/(Ar + He)$ are then carried out. The normalised isotopic transient concentrations obtained from on-line spectrometry data are reported in Fig. 6. Within the uncertainties of the MS resolution, no significant delay is observed between the CO_2 and the inert (He) transient curves. This means that under reaction conditions, the equilibrium which was previously observed between gaseous CO_2 and surface carbonates in the absence of methane is largely displaced towards an irreversible activation of CO_2. In contrast, a marked delay is observed for the CO transient curves. Integrating the shift between CO_2 and CO curves leads to an average residence time of the CO precursors on the surface of about 7.7 s. If one considers the CO_2-to-CO pathway as a first-order and irreversible reaction, an evaluation of the CO precursors can be obtained from the product of the rate of CO production (about 29 μmol/s/g_{cat} under the prevailing conditions) by the above average residence time (7.7 s), which gives a

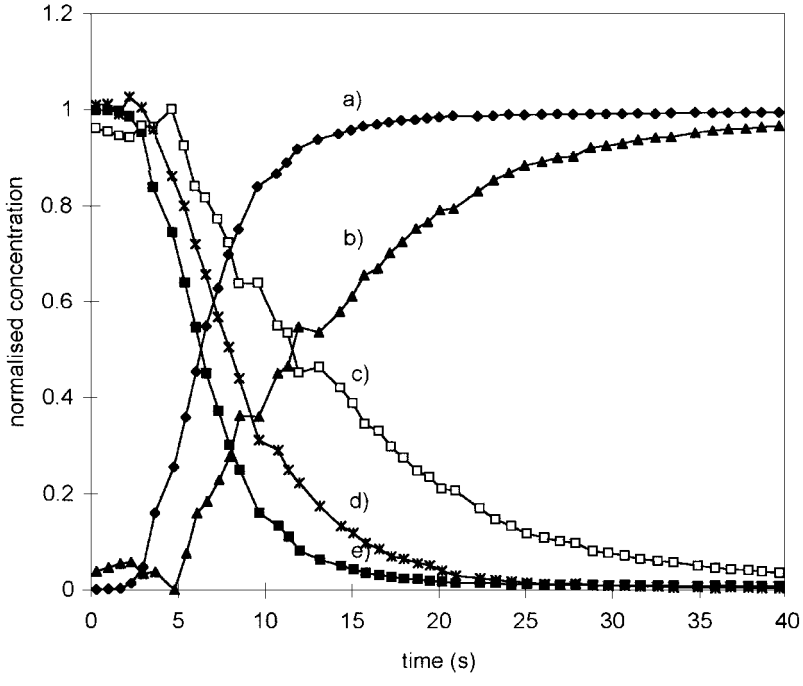

FIG. 6. Normalised changes in the isotopic concentration of the gas effluents after the $^{13}CO_2/^{12}CH_4$/Ar/He-to-$^{12}CO_2/^{12}CH_4$/Ar switch at 800°C: (a) $^{12}CO_2$; (b) ^{12}CO; (c) ^{13}CO; (d) He; (e) $^{13}CO_2$.

value of 225 μmol/g_{cat} (7, 8). This value compares quite well to the amount of exchangeable carbonate (300 μmol/g_{cat}) determined by transient DRIFT spectroscopy.

3.3. *TAP Experiments*

The $^{12}CH_4/^{13}CO_2$ pump-probe experiment consists in pulsing at 600°C in an alternating mode $^{12}CH_4$ and then $^{13}CO_2$ pulses of similar content (around 10^{16} molecules) over the Ni/La_2O_3 catalyst in a reduced state in order to get information concerning the reactive adspecies. The responses of this experiment are shown in Fig. 7b and compared to the responses obtained with a 4% Ni/SiO_2 under similar operating conditions (Fig. 7a from (8)). For Ni/La_2O_3 the conversion of methane and carbon dioxide amounts to 85 and 95%, respectively (87 and 96% for Ni/SiO_2).

For Ni/SiO_2 (Fig. 7a), hydrogen is produced almost instantly on the methane pulse, and the surface of the H_2 pulse indicates a complete cracking of the converted methane into H_2 and surface carbon. Two distinct carbon monoxide responses, but with close surface area, are observed together with the carbon dioxide pulse: (i) one corresponding to labelled ^{13}CO, almost concomitant with the unconverted labelled $^{13}CO_2$ and without tailing; (ii) another one corresponding to unlabelled ^{12}CO, markedly delayed and presenting a long tailing. Variations of the time-interval between the two pulses do not influence the spectra.

For Ni/La_2O_3 (Fig. 7b), a completely distinct picture is observed. Hydrogen is also produced on the methane pulse, but with a very long tailing, slightly decreasing upon the CO_2 pulse. Both ^{12}CO and ^{13}CO are almost continuously produced along the pump/probe experiment, except during the methane pulse, where the CO's production is stopped, and after the $^{13}CO_2$ pulse, where the production of both CO's is enhanced, before returning to a stationary rate of production. The two CO's responses present very close shape all along the experiment. Their intensities, slightly different in Fig. 7b (about 1.2 times more ^{12}CO than ^{13}CO), were found getting closer and closer by increasing the time of $^{13}CO_2$ pulsing period. A slight signal of $^{13}CO_2$ (and to a minor extent of $^{12}CO_2$) is also detected all along the experiment.

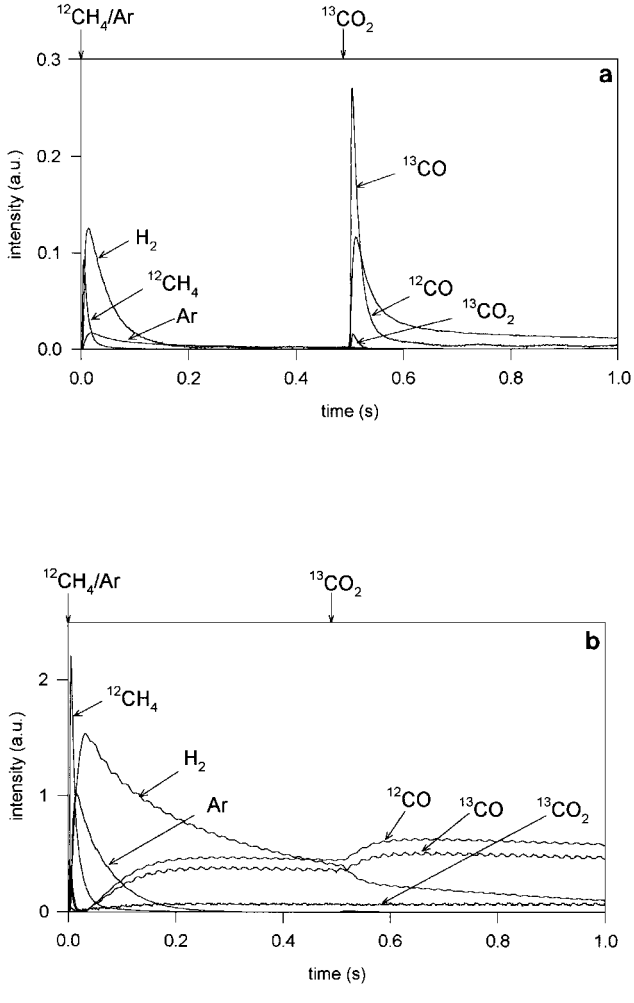

FIG. 7. TAP pump-probe pulse responses using $^{12}CH_4$ and $^{13}CO_2$ at 600°C over (a) Ni/SiO_2 (from [8]) and (b) Ni/La_2O_3.

4. DISCUSSION

The main features demonstrated in the present study are the following:

(i) As shown by TEM/EDX, a tight interface develops between the nickel and the lanthana phase after reduction by means of a thin layer (about 2 nm) which decorates the nickel particles. This interface is still directly observed after a short period of catalyst ageing. After a long period (20 h), large amounts of carbon deposits prevent any precise EDX evaluation of the nickel particle composition. However, the average particle size remains similar which suggests that no major changes in the catalyst morphology occur under reaction conditions. The only noticeable change concerns the few nickel particles extracted from the lanthana support by carbon filaments which are no more decorated by lanthanum-based material. During coke elimination by calcination at 750°C, a thorough sintering process occurs and solid/solid reactions tend to form mixed oxides, La_2NiO_4 and $LaNiO_3$. This observation indirectly confirms that the tight interaction which is observed on the fresh catalyst between the nickel particles and the lanthana support is maintained for most particles under the reaction conditions.

(ii) the existence of a pool of carbonate species at 700–800°C under a partial pressure of CO_2 which corresponds to the reforming conditions is directly and unambiguously revealed by isotopic transient DRIFT experiments. These species, mostly dioxomonocarbonate $La_2O_2CO_3$ are in fast equilibrium with the carbon dioxide in the gas phase. By modelling the transient curves, an amount of about 300 μmol/g_{cat} is calculated, which would represent the

TABLE 2

Surface Area of Nickel (Calculated from Ni Content and Dispersion) and Amount of CO Precursors (Deduced from SSITKA) for Ni/La_2O_3 and Ni/SiO_2 (Data from [3])

Catalyst	Ni content (wt%)	S_{Ni} (m^2/g_{Ni})	S_{Ni} (m^2/g_{cat})	Amount of CO precursors ($\mu mol/g_{cat}$)
Ni/La_2O_3	17	6	1.0	225
Ni/SiO_2	4	106	4.3	38

carbonatation of about 1/10 of the lanthana support, i.e. more than 20 layers of the oxide particles. A rough evaluation of the amount of lanthanum oxide (or carbonate) which decorates the nickel particles leads to a value of the same order of magnitude as the above determined pool of carbonates.

(iii) SSITKA experiments reveal that under steady-state reforming conditions, the equilibrium between gaseous CO_2 and adsorbed CO_3^2 species is strongly displaced towards an irreversible activation of CO_2. A second key mechanistic information is that a large pool of CO precursors exists on the catalytic surface as shown by the delay observed for the isotopic transients of gaseous CO. The calculated amount of these precursors is compared in Table 2 to the results obtained on a Ni/SiO_2 catalyst under similar operating conditions (3).

For the case of Ni/SiO_2, both CH_4 and CO_2 activations are assumed to occur directly on the metallic surface (3). The measured accumulation of CO precursors is assigned to the carbon adspecies issued from methane cracking and to the oxygen adspecies issued from CO_2 dissociation into O and gaseous CO. The following scheme summarises the related elementary steps:

$$CH_4 + Ni \rightleftarrows NiC + 2H_2 \quad [1]$$

$$CO_2 + Ni \rightleftarrows CO + NiO \quad [2]$$

$$NiC + NiO \rightarrow CO + 2Ni \quad [3]$$

Note that within the step [1], the intermediate formation of hydrogenated species CH_x and a fast gas/surface hydrogen equilibrium have to be considered in order to account for the observed H/D exchange reactions (3). Thus, step [1] can be considered under the present conditions as a fast step lumping several elementary steps, largely reversible at 750°C and leading to the accumulation of dehydrogenated carbon monomers.

Step [3] is assumed to be rate determining, in agreement with the absence of H/D isotopic effects (3).

For the present case of Ni/La_2O_3, such a mechanistic scheme does not apply anymore since a much larger accumulation of CO precursors is observed for a lower available surface of nickel (Table 2). This large accumulation of CO precursors is also directly observed in the TAP pump-probe experiment with the continuous production of CO's before and after the pulses of gaseous reactants (Fig. 7b). A rather good correspondence is found between the amount of CO precursors (225 $\mu mol/g_{cat}$) and the amount of lanthanum carbonates in equilibrium with the CO_2 atmosphere (300 $\mu mol/g_{cat}$). The storage of CO precursors outside the nickel surface, in the form of lanthanum carbonate, can therefore be postulated, as initially proposed by Zhang *et al.* (4, 5). The TAP experiment also reveals that the CO production is inhibited during the methane pulse, i.e. during methane cracking on the metallic nickel, step [1′]. This could mean that the lanthanum carbonate decomposition into CO occurs on nickel metal, in competition with the methane cracking. Thus, the mechanistic scheme on Ni/La_2O_3 can be proposed as

$$CH_4 + Ni \rightarrow NiC + 2H_2 \quad [1']$$

$$La_2O_2CO_3 + Ni \rightarrow CO + NiO + La_2O_3 \quad [2']$$

$$NiC + NiO \rightarrow CO + 2Ni \quad [3']$$

$$CO_2 + La_2O_3 \rightarrow La_2O_2CO_3. \quad [4']$$

The similarity in curve shapes observed in Fig. 7b for the unlabelled and labelled CO responses tends to indicate that steps [2′] and [3′] are fast and solely controlled by the surface concentration of sites. Step [4′] of the carbonate regeneration is shown to be in equilibrium under CO_2 atmosphere (Fig. 4), but essentially irreversible under steady-state reaction conditions since no accumulation of reversible CO_2 is detected upon SSITKA experiment in Fig. 6 (no delay between He and CO_2 responses). However, under the TAP pump-probe conditions (very low partial pressure of CO_2), a continuous residual flux of CO_2 attests of the reverse decomposition of carbonates. In any case, this step is also likely to be a fast step. Note that the larger production of ^{12}CO compared to ^{13}CO in Fig. 7b simply derives from the fact that the carbonate pool was not yet completely exchanged with ^{13}C during the reported pump-probe experiment. As a matter of fact, the production of CO's tends to be closer and closer by completing the carbonate pool isotopic exchange.

At variance with the case of Ni/SiO_2, it can be deduced from the above scheme that the step [3′] cannot be considered anymore as rate determining. This renders very likely that the step [1′] of methane cracking is now rate determining. The latter would include the elementary steps involved in the step-wise dehydrogenation of methane, which would increase the surface concentration of hydrogenated species, as deduced from the long tailing of the H_2 TAP response in Fig. 7b. This statement is in perfect agreement with the observation of a kinetic isotopic effect (KIE) reported earlier over the same Ni/La_2O_3 catalyst (13); a reduction of the rate of CO formation by a factor of 1.19–1.97 (which corresponds to the expected KIE at this temperature when a C–H

or H−H bond activation is involved in a rate-determining step) was observed upon switching the feed from CH_4/CO_2 to CD_4/CO_2. A plausible explanation for this specific mechanistic feature is that the decoration of the nickel particles by the lanthana phase would hinder the methane cracking on the nickel surface and the recombination of surface hydrogen atoms into H_2 molecules.

The question arises now to determine if the specific configuration of the active phase and the above mechanistic features observed for the Ni/La_2O_3 catalyst may explain its unique resistance to deactivation (5, 6). Among the different types of coke deposits formed during the methane reforming, it was shown in a previous study on Ni/SiO_2 (2) that the carbon filaments which keep alive the Ni particles extracted from the support by the growing filaments do not deactivate the catalyst directly, except after a massive accumulation finally plugging the reactor and/or by a progressive fragmentation of the particles and/or by encapsulation of the particles in filament nodes. In contrast, the deactivating coke was identified as a polymorphic form of graphite which develops as veils around the particles and tends to encapsulate them, therefore limiting or suppressing the access of reactants to the metal surface and the products desorption (2).

The first observation is that the formation of carbon whiskers was shown to occur on this catalyst as for any type of reforming catalyst, but to a limited extent. This could delay the ultimate effect of reactor plugging or nickel particle fragmentation. The second and possibly the main positive effect could be directly related to the catalyst morphology; the tight coating of the nickel particles by the layer of lanthanum carbonate would hinder the formation of deactivating coke, possibly by limiting the carbon migration through the nickel particles (due to the long residence time of hydrogen species at the interface) and its recombination as an encapsulating veil around the particle.

5. CONCLUSION

At variance with the "mono functional" mechanism proposed over Ni/SiO_2, a "bifunctional" mechanism is proposed over Ni/La_2O_3 to account for the specific features revealed by transient kinetic experiments combined with a TEM/EDX investigation. The existence of a thin overlayer of lanthana on top of the nickel particles creates a tight interface between two active phases. The lanthana phase, easily carbonated by gaseous CO_2 acts as a continuous supplier of gaseous CO and activated oxygen in contact with the nickel phase. The latter oxygen species reacts with the surface carbon arising from the methane cracking over the nickel phase, thus providing a second source of gaseous CO. A quantitative evaluation of the reacting intermediates is provided in good agreement with the catalyst morphology. This specific morphology of the active phase is also assumed to hinder the formation of deactivating coke, which explains the unique catalytic stability of such a formula.

ACKNOWLEDGMENTS

Thanks are due to M. T. Gimenez for XRD analysis, to EU (HCM programme) and to Rhône-Alpes District Council for granting a large part of this work.

REFERENCES

1. Slagtern, Å., Olsbye, U., Blom, R., Dahl, I. M., and Fjellvåg, H., *Appl. Catal. A: General* **145**, 375 (1996).
2. Kroll, V. C. H., Swaan, H. M., and Mirodatos, C., *J. Catal.* **161**, 409 (1996).
3. Kroll, V. C. H., Swaan, H. M., Lacombe, S., and Mirodatos, C., *J. Catal.* **164**, 387 (1996).
4. Zhang, Z. L., and Verykios, X. E., *Appl. Catal.* **138**, 109 (1996).
5. Zhang, Z. L., Verykios, X. E., MacDonald, S. M., and Affrosman, S., *J. Phys. Chem.* **100**, 744 (1996).
6. Zhang, Z. L., and Verykios, X. E., *J. Chem. Soc. Chem. Commun.*, 71 (1995).
7. Mirodatos, C., *Catal. Today* **9**, 83 (1991).
8. Schuurman, Y., and Mirodatos, C., *Appl. Catal.* **151**(1), 305 (1997).
9. Gleaves, J. T., Ebner, J. R., and Kuechler, T. C., *Catal. Rev.-Sci. Eng.* **30**, 49 (1988).
10. Lacombe, S., Geantet, C., and Mirodatos, C., *J. Catal.* **151**, 439 (1995).
11. Soong, Y., Krishna, K., and Biloen, P., *J. Catal.* **97**, 330 (1986).
12. Happel, J., Walter, E., and Lecourtier, Y., *J. Catal.* **123**, 12 (1990).
13. Zhang, Z. L., and Verykios, X. E., *Catal. Lett.* **38**, 175 (1996).